Multinary alloy electrodes for solid state batteries II. A new Li–Si–Mg alloy negative electrode material for use in high energy density rechargeable lithium cells

A. Anani* and R. A. Huggins
Department of Materials Science and Engineering, Stanford University, Stanford, CA 94305 (USA)

(Received September 4, 1991; in revised form December 12, 1991)

Abstract

Electrochemical coulometric titration has been used to explore the electrode properties of a ternary Li–Si–Mg alloy composition. The measured electrode potential and lithium capacity for this system are comparable to those estimated from consideration of the isothermal Gibbs triangle for the ternary system. These measured values are far higher than those of the state-of-the-art binary systems currently employed in thermal batteries. For example, measured electrode potentials for the ternary alloy at 440 °C were about 90 mV more negative than those for the conventional 44 wt.% Li–Si binary alloy, translating to a loss of only about 70 mV compared to pure lithium. Consequently, the maximum specific energy (considering active materials only) of a cell employing this material as the negative electrode component with a hypothetical cathode (say, one lithium in 60 g of active material) which is 2.0 V positive of pure lithium should be about 35% higher than that of a comparable cell using the 44 wt.% Li–Si binary alloy.

Introduction

The many and varied requirements of a battery and the different electrical and environmental conditions under which they must operate necessitate the manufacture and use of a number of different types of cells with varying designs. Reversible lithium batteries with high energy (and power) density as well as high specific energy (and power) fall into one of these categories of cells as interest in finding better methods for energy storage increases. Applications such as power sources for electric vehicles and stationary energy storage for load levelling in power plants are envisioned for these lithium battery systems.

The cycling behavior of lithium-based electrochemical cells, however, is often limited by problems associated with the negative electrode. In the case where elemental lithium is employed as the negative electrode, these problems may include gradually increased interfacial impedance caused by the formation of ionically blocking reaction product layers from the reaction between the electrode and species in the electrolyte. This is an endemic problem with the use of organic solvent electrolytes with elemental

*Author to whom correspondence should be addressed. Present address: Center for Electrochemical Systems and Hydrogen Research, Texas A&M University, College Station, TX 77843, USA.

0378-7753/92/$5.00

lithium electrodes at ambient temperatures. The presence of such layers, and the local nature of their electrical breakdown, generally related to defects in their structure, often causes the formation of deleterious filamentary and dendritic growth upon recharge. This may in turn lead to electrical shorting between the electrodes and may also isolate active electrode materials from electrochemical reactions, resulting in severe loss of capacity.

At elevated temperatures where lithium is a liquid, these problems may also include corrosion, stability and difficulty in containment. Another problem is the fact that alkali metals dissolve in their halides, and thus in lithium cells, dissolution of lithium in its molten halide salt electrolyte would lead to electronic leakage in the electrolyte causing severe self-discharge.

These problems can often be reduced by using lithium alloys instead of pure lithium as the negative electrode reactant. Since the melting point of alloys is often higher than that of pure elements, the electrode, in most cases, will remain solid to higher temperatures. This can be important for safety reasons in situations in which local heating might otherwise cause melting.

In the absence of a significant nucleation barrier, deposition of elemental species will tend to occur anywhere at which the electric potential is such that the element's chemical potential is at or above that corresponding to unit activity. This means that electrodeposition may take place upon current collectors and other parts of the electrochemical cell that are at the same potential as the negative electrode, as well as upon the electrode structure where it is actually desired. Alloy electrodes with fast kinetics provide this inherent barrier by virtue of the fact that the activity of the electroactive species never gets to unity at the electrode surface. Deposition of the electroactive species therefore occurs preferentially upon the desired electrode structure rather than at other undesired locations in the cell. As a consequence also, dendrite formation, and in favorable cases, formation of deleterious surface films, are avoided by the use of alloy electrodes.

Several alloys have been investigated for use at both elevated temperatures [1–9] and ambient temperatures [10–16]. At elevated temperatures, the two-phase alloys in the Li–Al [1, 2] and Li–Si [7, 8] systems which function at voltages only slightly less negative than that of molten lithium are currently being used in practical cells. That the reversibility and cycle life of electrochemical cells can generally be increased by the use of such alloy electrodes, is not to imply that they are without their own shortcomings. For instance, their use implies reductions in the associated specific energy and energy density. These are a consequence of the reduced activity of the electroactive species in the negative electrode, which implies reduced cell voltage, as well as increased weight. Other drawbacks many include volume and shape changes as well as material property to function as a mixed-conductor without the addition of other components. There is therefore the need for a continued search for alloy electrodes that will lead to cells with improved characteristics.

In a previous publication [17], the theory and methodology for screening ternary and quaternary alloy materials for use as the active negative electrode components in lithium cells were described. In particular, the method described how the addition of a third component to a binary system will affect thermodynamic properties such as electric potential, capacity and thus energy of the original system. This was further applied to several Li–Si-based ternary systems. In some cases, more than a two-fold factor change in the predicted capacity and energy was observed. The properties of three compositions, one each from the addition of Ca, Mo and Mg, were much higher than their Li–Si binary alloy counterpart.

The present communication reports on the results of experimental verification of the Li–Si–Mg ternary system. These results are compared with those from the thermodynamic predictions in order to establish the strength and versatility of the technique.

Experimental

Materials and materials preparation

The starting material for the Li–Si–Mg system experiments, Mg_2Si(98%), was obtained from Morton Thiokol, Inc. (Alfa products). The LiCl–KCl eutectic, used as electrolyte was from Lithium Corporation of America, while the 44% Li–Si alloy was from Sandia National Laboratory. Additional purification of the molten LiCl–KCl eutectic electrolyte was required in order to remove any residual trace of water that would otherwise react with the lithium alloys. The purification process involves successive use of elemental lithium and aluminium to remove traces of water and residual lithium, respectively. Electrode samples were made by cold pressing the appropriate powder into pellets. No additive was used as current collector since the alloys were themselves electronically conducting.

Experimental procedure

The three electrode galvanic cell arrangement used in the experiments can be represented by

(−) 44% Li–Si alloy/LiCl–KCl eutectic/Li_xMg_2Si (+) (I)

with the 44% Li–Si alloy (Li:Si ratio = 3.18) as the reference electrode. The operating temperature was held at about 440 °C. Both dynamic and equilibrium open circuit measurements were controlled using a potentiostat/galvanostat (PAR, model 173) coupled with a digital coulometer (PAR, model 179). Potentials were monitored through a digital multimeter (Keithley, model 172) and chart recorder arrangement.

All experiments and materials preparations were carried out in a helium-filled glove box.

Results and discussion

Predicted thermodynamic properties of the Li–Si–Mg ternary system

The equilibrium isothermal Gibbs triangle for the Li–Si–Mg system at 400 °C obtained from consideration of the free energies of all the phases present in the system is shown in Fig. 1. In addition to the basic thermodynamic equilibria in the binary Li–Si system [18], and marked A to D in Fig. 1, there is a prominent equilibrium three-phase tie-triangle which is introduced as a result of the addition of magnesium. This three-phase, Mg_2Si–Mg–$Li_{13}Si_4$, equilibrium identified by I in Fig. 1 can be represented by the reaction:

$$4Mg_2Si + 13Li \rightleftharpoons 8Mg + Li_{13}Si_4 \quad (1)$$

If a hypothetical electrode is made from an alloy of composition Mg_2Si, then upon discharge, i.e. on addition of lithium to the electrode, the composition of the electrode, and thus the lithium activity and electrode potential, will move from Mg_2Si towards lithium, crossing regions of both three-phase and two-phase equilibria following the

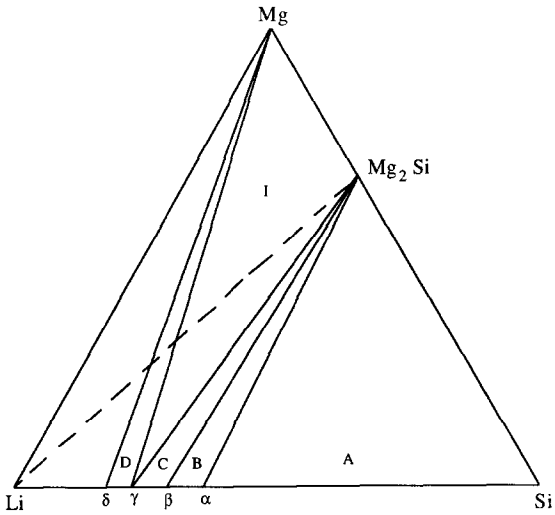

Fig. 1. Equilibrium isothermal phase diagram for the Li–Si–Mg ternary phase diagram estimated at 400 °C. α, β, γ and δ represent the Li–Si binary phases $Li_{12}Si_7$, Li_7Si_3, $Li_{13}Si_4$ and $Li_{22}Si_5$, respectively.

path indicated by the dotted line in the phase diagram. In the tie-triangle marked I, and according to reaction (1), the Gibbs free energy change of the reaction is calculated to be −18.008 kcal and the corresponding electrode potential is 60 mV positive of pure lithium. The theoretical lithium capacity for this composition is 876 A h/kg. Upon intergration of the difference between the electrode potential and that of a hypothetical positive cathode such as FeS_2 say, which is 2.0 V versus pure lithium over all available capacity, one obtains a maximum theoretical specific energy of 574 W h/kg of active electrode components. Thermodynamic properties predicted for the Li–Si–Mg system are compared with those of a reference 44 wt.% Li–Si binary alloy electrode in Table 1. In this comparison, it is shown that the lithium storage capacity of a conventional Li–Si binary alloy electrode can be increased by an estimated 80% with the use of a ternary Li–Si–Mg alloy. This increment translates to a 34% increase in the maximum specific energy of a cell utilizing this ternary alloy material as the active electrode component.

Experimentally measured properties for the Li–Si–Mg ternary system

Figure 2 shows a typical dynamic electrode potential versus time plot obtained from an 'as received' Mg_2Si sample during galvanostatic addition of lithium at a current density (geometric) of 10 mA/cm^2. The potentials have been converted to potentials versus pure lithium using the open circuit voltage versus temperature plot for the appropriate Li–Si binary plateau region reported by Sharma and Seefurth [5]. Four plateau regions are easily identifiable, with the most interesting occurring at about 49 mV positive of pure lithium. This is exactly what is predicted from the Li–Si–Mg ternary phase diagram if one were to start from Mg:Si ratio slightly richer in Si than the Mg_2Si phase. In this case, four plateau voltages would be identified, the first three corresponding to potential plateaus A, B and C in the Li–Si binary system, and the fourth to the three-phase equilibrium identified by I in the phase diagram of

TABLE 1

Comparison of theoretical and experimental thermodynamic properties of a ternary Li–Si–Mg alloy electrode with those of the 44 wt.% Li–Si binary alloy

System	Electrode potential (mV vs.Li)	Electrode capacity		Specific energy of cell[a] (W h/kg)
		Li/kg	A h/kg	
Li–Si				
Li_7Si_3–$Li_{13}Si_4$	158	18.1	485	428
Li–Si–Mg: prediction				
Mg_2Si–Mg–$Li_{13}Si_4$	60 (98)	32.7	876 (81%)	574 (34%)
Li–Si–Mg: experimental				
$MoSi_2$–Mo_5Si_3–$Li_{13}Si_4$	70 (88)	29.4	788 (62%)	513 (20%)

Numbers in parentheses represent improvements over conventional Li–Si binary alloy. [a]Specific energy $= \frac{\int_{\text{capacity}} (\text{cell voltage})}{\text{weight}}$ where cell voltage = potential difference between alloy electrode and hypothetical positive electrode and hypothetical positive electrode defined in text.

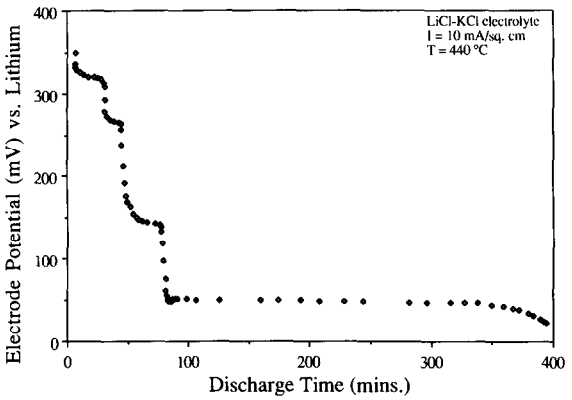

Fig. 2. Typical dynamic curve during lithium addition to the 'as-received' Mg_2Si sample at a current density (geometric) of 10 mA/cm^2.

Fig. 1. Therefore in Fig. 2, the plateaus at 320, 265 and 144 mV positive of pure lithium represent reactions of lithium with pure silicon according to the Li–Si binary system, with the Mg_2Si phase acting purely as a matrix for the Li_xSi reactant. There is no observable reaction of lithium with Mg_2Si during this time. However, in the fourth plateau region, the Mg_2Si phase becomes the reactant while the final Li–Si phase formed in course of the binary Li–Si reaction, $Li_{13}Si_4$, acts as the matrix phase. The rate of lithium diffusion in the $Li_{13}Si_4$ phase has been determined by Wen and Huggins [18], reporting a composition dependent diffusion coefficient with values in the range of 7.00×10^{-5} to 9.33×10^{-5} cm^2/s. These numbers are comparable to diffusion coefficients in liquid phases. Following the arguments for the mixed conduction matrix concept [19–22], it is therefore not surprising that one sees evidence of fast kinetics

in the Li–Si–Mg system. That is, in the plateau region of interest, the $Li_{13}Si_4$ phase acts as a host for the Li_xMg_2Si reactant. Evidence for fast kinetics (as will be shown later) can be seen in these systems by the sharp rise in the potentials to steady state values upon current interruption. Also, the potential plateau regions appear flat during dynamic galvanostatic charging or discharging of the electrode. This does not seem to change much even at higher current densities.

Figure 3 shows the performance of the electrode sample upon repeated cycling, in terms of the cell voltage versus capacity utilization at different current densities. These plots were recorded during the twentieth cycle. Both the flatness of these discharge/charge curves and their relatively small sensitivity to current indicate fast kinetics in the sample electrode.

At the onset of a discharge or charge process, a small voltage spike is observed. Such spikes are normally associated with the nucleation of new phases as the addition or removal of the electroactive specie moves the equilibria from one tie-triangle to another. During lithium addition into this system, the new phases formed are Mg and $Li_{13}Si_4$, and upon complete convertion, the Mg_2Si phase is nucleated during the reverse process, i.e. during lithium removal. After nucleation, subsequent phase formation is by a growth process. The spike height represents a relative measure of the activation energy barrier that has to be overcome in order for nucleation of the new phase to occur. The spike heights are small for this system, and remain constant with current density. Because of the low activation energy for nucleation in this system, reversibility during charge and discharge processes does not seem to constitute a problem. Hence, the entire range of capacity for the system can be explored with relative ease. On the other hand, though, the voltage spike is readily avoidable if they present any experimental hindrance to the performance of the electrode. To do this, the starting electrode material should be fabricated in such a way as to include a minute amount of the nucleated phase(s) in the starting composition. In addition, discharge and charge cycles should be terminated before reaching the ends of the three-phase equilibrium. This way, all three phases will always be present in the reactant sample.

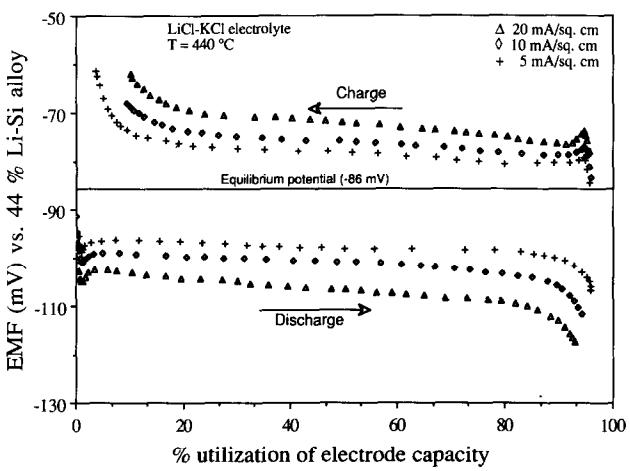

Fig. 3. Cycling characteristics of the Mg_2Si-based electrode operated within the three-phase Mg_2Si–Mg–$Li_{13}Si_4$ tie-triangle. Plot shows the electrode performance after the twentieth cycle at three different current densities.

A qualitative measure of the electrode's capacity retention capability is also illustrated in Fig. 3. Although the cycle numbers attained here are considerably low compared to what is expected for a long-life battery, they represent an excellent preliminary measure of battery characteristics on a laboratory scale. At current densities as high as 20 mA/cm^2, over 90% of the theoretically available electrode capacity could still be utilized without any appreciable deviation of the electrode potential from the onset value. The utilization is slightly higher at lower current densities. For this sytem, considering the theoretical capacity as the C value, a charge or discharge rate of 20 mA/cm^2 will be equivalent to a 0.36 C (or C/2.7) rate.

The deviation of the dynamic cell voltage from the measured equilibrium potential is shown in Fig. 4 as a function of the current density. The polarization is shown for a 50% state of capacity utilization. The polarization resistance values, of the order of 0.40 and 0.57 mV/mA cm^{-2} of geometric surface area for the charge and discharge cycles, respectively, are considered small at these current densities and temperature. They become only slightly higher near the end of the discharge and charge cycles. The deviation of the polarization voltage from the equilibrium potential value at zero current represents the internal resistance loss in the cell which is not corrected for in this plot. The difference in the polarization and thus in the resistance during charge and discharge is due possibly to the nucleation and growth of totally different phases on the outer surface of the electrode during the different processes giving rise to a slight difference in the surface impedance.

Equilibrium open circuit measurements as a function of composition were obtained by measurements on several individually prepared samples with compositions that lie along the dotted line joining the Mg_2Si phase to the lithium corner of the phase diagram, Fig. 1. Measurements were also made by coulometric titration of lithium into Mg_2Si to comparable compositions estimated from the amount of charge passed. The results of both of these sets of experiments are shown in Table 2 as electrode potentials versus lithium, and compared to those predicted from thermodynamic considerations. The electrode potential values shown for both the 'as-prepared' and 'coulometrically titrated' compositions are average values for five and four different

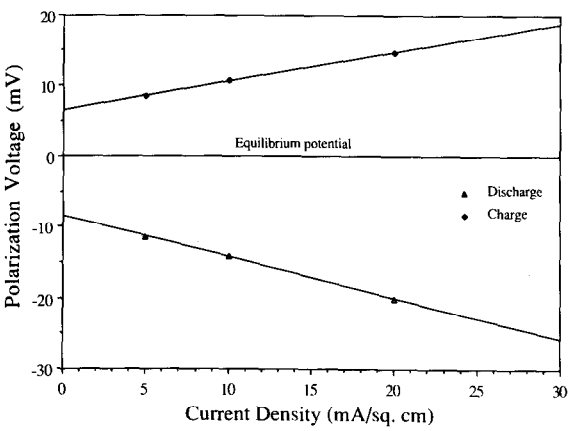

Fig. 4. Polarization characteristics of the cell: (−) 44% Li–Si alloy/ LiCl–KCl eutectic/Li_xMg_2Si (+) at 440 °C. The polarization behavior was measured as the deviation of the dynamic electrode potential from equilibrium at 50% capacity utilization.

TABLE 2

Comparison between 'theoretical estimated' and 'experimentally measured' equilibrium potentials for different compositions in the Mg_2Si–Mg–$Li_{13}Si_4$ equilibrium

	'As prepared' compositions	'Coulometrically titrated' compositions	Thermodynamic estimation
mV vs. Li	69[a]	70[b]	60
mV vs. 44 wt.% Li–Si (+158 mV vs. Li)	−89	−88	−98

[a]Averaged over five distinct compositions.
[b]Averaged over four distinct compositions.

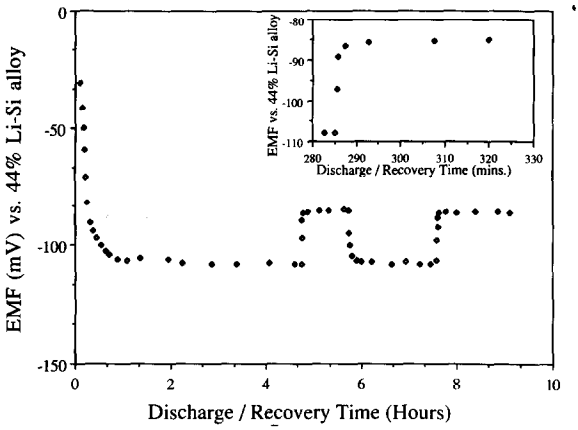

Fig. 5. Typical discharge (lithium addition) and recovery curve for a composition in the Mg_2Si–Mg–$Li_{13}Si_4$ three phase tie-triangle. The insert is an expansion of a recovery portion in the main plot.

compositions corresponding to x in Li_xMg_2Si values of 0.45, 1.00, 1.54, 2.56 and 3.25 and 0.75, 1.11, 1.35 and 2.26, respectively. In general, the experimentally measured potentials are a few millivolts higher than those predicted, but within an acceptable range, considering the difference in temperature between the two (i.e. temperature of the measurements and temperature at which the predictions were made), and the lack of knowledge of the precision of the thermodynamic data.

One technique commonly used to observe and qualitatively measure equilibrium electrode potentials is the dynamic relaxation technique [23]. In this technique, an electrode in its partially charged or discharged state is held at open circuit while the potential is allowed to recover to a steady state value. Phase changes as well as phases in equilibrium are represented by regions of changing potentials with time and constant plateau potentials, respectively, in the relaxation curve, while the eventual steady state potential represents the equilibrium electrode potential for the given state of charge. Results of experiments based on the relaxation technique, however, not only lead to measured values of the steady state potentials, they also demonstrate the coulometric titration technique, a tool which was used extensively in this work. Figure 5 is a typical

discharge and recovery curve for a composition in the Mg_2Si–Mg–$Li_{13}Si_{14}$ three-phase tie-triangle. The average equilibrium potential for successive discharge–recovery cycles, measured in the tie-triangle using this technique is −86 mV versus 44 wt.% Li–Si alloy, or equivalently, +72 mV versus lithium. This value is comparable to those listed in Table 2. The insert in Fig. 5 is an expansion of a recovery portion in the main curve to show the sharp rise time which could easily be viewed as a relative measure of the kinetics in the electrode material structure.

The lithium-rich limit of the three-phase equilibrium represented by reaction (1) was determined by adding and deleting small amounts of charge to a sample of composition corresponding to the intersection of the dotted line joining the Mg_2Si phase to the lithium-rich corner and the $Li_{13}Si_4$–Mg tie-line. Two potential plateau regions were observed. The voltages of these plateaus correspond to those of the Mg_2Si–Mg–$Li_{13}Si_4$ and $Li_{13}Si_4$–$Li_{22}Si_5$ equilibria. This observation establishes the validity of the ternary phase diagram, Fig. 1, and thus confirms the theoretical capacity of the Mg_2Si–Mg–$Li_{13}Si_4$ three-phase equilibrium as predicted from thermodynamic considerations, at 876 A h/kg of active material. The lithium capacity for this triangle was compared with those of the reference Li_7Si_3–$Li_{13}Si_4$ equilibrium in Table 1. Experimentally, upto 90% of this capacity can be utilized during charge and discharge cycling. Using this actual utilization value of the electrode capacity and the measured electrode potential, the specific energy for a cell utilizing this electrode with the same reference cathode as before is 513 W h/kg. This value represents a decrease of only 10% of the theoretical value. Experimentally measured and derived thermodynamic properties for this ternary system are also compared with those predicted from thermodynamic considerations in Table 1.

Conclusions

The influence of the addition of magnesium to the binary Li–Si system has been evaluated using isothermal phase diagrams, with the result that an additional three-phase constant potential plateau was introduced. The estimated thermodynamic parameters for this tie-triangle include a lithium capacity of 876 A h/kg and a potential of only +60 mV versus elemental lithium. These values are to be compared with 485 A h/kg and +158 mV versus pure lithium, respectively, for the Li_7Si_3–$Li_{13}Si_4$ binary alloy composition.

Electrochemical coulometric titration techniques were employed to establish phase equilibrium tie-lines as predicted from the isothermal phase diagrams. The electrode potential measured for the Mg_2Si–Mg–$Li_{13}Si_4$ three-phase equilibrium was about +70 mV versus lithium. During charge/discharge cycling of an electrode from this tie-triangle upto the twentieth cycle, over 90% of the available capacity was utilized. For a given reference cathode, these measured values of potential and capacity convert to a maximum specific energy of 513 W h/kg which is within 10% of the theoretically estimated value. Based on these measurements, it is further estimated that a cell employing this ternary alloy as the negative electrode reactant should have a specific energy which is about 35% higher than that for a comparable cell employing the Li_7Si_3–$Li_{13}Si_4$ binary alloy which is the active material in the present-day thermal batteries.

Acknowledgement

Financial support for this work has been provided by Sandia National Laboratory under contract No. 53-3321.

References

1 N. P. Yao, L. A. Heredy and R. C. Saunders, *J. Electrochem. Soc., 118* (1971) 1039.
2 E. C. Gay, D. R. Visers, F. J. Martino and K. E. Anderson, *J. Electrochem. Soc., 123* (1976) 1591.
3 L. R. McCoy and S. Lai, in *Proc. Symp. and Workshop Advanced Battery Research and Design,* Argonne National Lab., ANL-76-8, 1976, p. B-167.
4 S. Lai, *J. Electrochem. Soc., 123* (1976) 1196.
5 R. A. Sharma and R. N. Seefurth, *J. Electrochem. Soc., 123* (1976) 1763.
6 C. J. Wen, *Ph.D. Dissertation,* Stanford University, 1980.
7 R. N. Seefurth and R. A. Sharma, *J. Electrochem. Soc., 124* (1977) 1207.
8 R. N. Seefurth and R. A. Sharma, *J. Electrochem. Soc., 127* (1980) 1101.
9 J. P. Doench and R. A. Huggins, *J. Electrochem. Soc., 129* (1982) 341C.
10 J. Wang, I. D. Raistrick and R. A. Huggins, *J. Electrochem. Soc., 133* (1986) 457.
11 J. Wang, P. King and R. A. Huggins, *Solid State Ionics, 20* (1986) 185.
12 Y. Toyoguchi, T. Matsui, J. Yamaura and T. Iijima, *3rd. Int. Meet. Lithium Batteries, Kyoto, Japan, May 27–30, 1986.*
13 B. M. L. Rao, R. W. Francis and H. W. Christopher, *J. Electrochem. Soc., 124* (1977) 1490.
14 R. D. Rauh, F. S. Shuker, J. M. Marston and S. B. Brummer, *J. Inorg. Nucl. Chem., 39* (1977) 1791.
15 M. Garreau, J. Thevenin and M. Fekir, *J. Power Sources, 9* (1983) 235.
16 T. R. Jow and C. C. Liang, *J. Electrochem. Soc., 129* (1982) 1429.
17 A. Anani and R. A. Huggins, *J. Power Sources, 38* (1992) 359–370.
18 C. J. Wen and R. A. Huggins, *J. Solid State Chem., 37* (1981) 271.
19 B. A. Boukamp, G. C. Lesh and R. A. Huggins, *J. Electrochem. Soc., 128* (1981) 725.
20 B. A. Boukamp, G. C. Lesh and R. A. Huggins, in H. V. Venkatasetty (ed.), *Proc. Symp. Lithium Batteries,* The Electrochemical Society, Pennington, NJ, 1981, p. 467.
21 R. A. Huggins and B. A. Boukamp, US Patent 4 436 769 (1984).
22 A. Anani, S. Crouch-Baker and R. A. Huggins, in A. N. Dey (ed.), *Proc. Symp. Lithium Batteries,* The Electrochemical Society, Pennington, NJ, 1987, p. 382.
23 C.-K. Huang, A. Anani, S. Crouch-Baker and R. A. Huggins, *170th Meet. Electrochemical Society, San Diego, CA, Oct. 19–24, 1986* Ext. Abstr. no. 96.